The Astrophysical Journal Supplement Series, 154:309–314, 2004 September

NEW INFRARED EMISSION FEATURES AND SPECTRAL VARIATIONS IN NGC 7023

M. W. Werner,[1] K. I. Uchida,[2] K. Sellgren,[3] M. Marengo,[4] K. D. Gordon,[5] P. W. Morris,[6] J. R. Houck,[2] and J. A. Stansberry[5]
Received 2004 March 20; accepted 2004 May 6

ABSTRACT

We observed the reflection nebula NGC 7023, with the Short-High module and the long-slit Short-Low and Long-Low modules of the Infrared Spectrograph on the *Spitzer Space Telescope*. We also present Infrared Array Camera (IRAC) and Multiband Imaging Photometer for *Spitzer* (MIPS) images of NGC 7023 at 3.6, 4.5, 8.0, and 24 μm. We observe the aromatic emission features (AEFs) at 6.2, 7.7, 8.6, 11.3, and 12.7 μm, plus a wealth of weaker features. We find new unidentified interstellar emission features at 6.7, 10.1, 15.8, 17.4, and 19.0 μm. Possible identifications include aromatic hydrocarbons or nanoparticles of unknown mineralogy. We see variations in relative feature strengths, central wavelengths, and feature widths, in the AEFs and weaker emission features, depending on both distance from the star and nebular position (southeast vs. northwest).

Subject headings: dust, extinction — infrared: ISM — ISM: individual (NGC 7023) — ISM: lines and bands — ISM: molecules — reflection nebulae

1. INTRODUCTION

The interstellar aromatic emission features (AEFs) at 6.2, 7.7, 8.6, 11.3, and 12.7 μm characterize the mid-infrared (mid-IR) emission of the diffuse interstellar medium (ISM) of our own and other star-forming galaxies. Duley & Williams (1981) first suggested that the AEFs were due to aromatic hydrocarbons. Léger & Puget (1984) and Allamandola et al. (1985) attributed the AEFs to polycyclic aromatic hydrocarbon (PAH) molecules with $\sim$50 carbon atoms. We present here *Spitzer Space Telescope* (Werner et al. 2004) images and spectroscopy of NGC 7023, a reflection nebula (RN) with AEFs, illuminated by the Herbig Be star HD 200775, at a distance of 430 pc (van den Ancker et al. 1997).

2. OBSERVATIONS

We imaged NGC 7023 with the Infrared Array Camera (IRAC; Fazio et al. 2004) in all four channels (3.6, 4.5, 5.8, and 8.0 μm) in two epochs (2003 October 10 and December 18). The images were reduced with the *Spitzer* Science Center (SSC) IRAC reduction pipeline and combined with the SSC mosaicker. This processing included dark subtraction, flat-fielding, mux-bleed correction, flux calibration, correction of focal plane geometrical distortions, and cosmic-ray rejection. Figures 1 and 2 (Plates 1 and 2) show our final images at 3.6, 4.5, and 8.0 μm.

We obtained images at 24, 70, and 160 μm with Multiband Imaging Photometer for *Spitzer* (MIPS; Rieke et al. 2004), in the scan map mode at medium rate. We covered $10' \times 30'$ at all three wavelengths. We reduced the MIPS images using the MIPS Instrument Team Data Analysis Tool (Gordon et al. 2004). The reduction of the 24 μm image (Fig. 2) followed preflight expectations, with a 10% uncertainty on the final absolute calibration. The 70 and 160 μm images will be presented in a later paper.

We measured the Short-High (SH) Infrared Spectrograph (IRS; Houck et al. 2004) spectrum (9.9–19.4 μm; $R = \lambda/\Delta\lambda = 600$) of NGC 7023 on 2003 September 19. We obtained Long-Low (LL) long-slit IRS spectra (14.0–32.9 μm; $R = 60$–130) at two positions on 2003 October 1. These observations occurred during the checkout phase of *Spitzer*, resulting in larger than normal uncertainties in the SH and LL absolute positions of $\pm 5''$. We observed the Short-Low (SL) long-slit IRS spectrum (5.1–15.1 μm; $R = 60$–130) of NGC 7023 on 2003 October 25. IRS was sufficiently checked out by this point, resulting in a much smaller absolute positioning for the SL data of $\pm 1''$.

The data were reduced and spectra extracted using Cornell IRS Spectroscopy Modeling Analysis and Reduction Tool (Higdon et al. 2004). The spectra were calibrated by applying the spectrum and model template of point source calibrator α Lac to the intermediate un-flat-fielded product of the SSC pipeline. We subtracted blank sky spectra only from the SH spectrum, observed as *Spitzer* cooled, to remove thermal emission from the then warm ($\sim$45 K) baffles of the telescope. All spectra were extracted from fixed pixel ranges over the slit, except for SH, where we extracted the spectrum from over the entire aperture.

Figure 2 shows that the SL slit intersects the filaments seen to the northwest of HD 200775. Our primary LL slit intersects both the northwest filaments and HD 200775 (Fig. 2). The SL slit crosses our secondary LL slit at position A, shown in Figure 2. We obtained the SH spectrum at position B, also marked in Figure 2.

3. RESULTS

We present our spectra of NGC 7023 in Figures 3, 4, and 5. Table 1 gives the central wavelengths and nebular positions at which we discovered new interstellar, spectrally resolved, emission features.

Figure 3*a* shows the combined SL and LL spectrum (5–33 μm) at position A. The absolute flux calibrations of SL1

[1] Jet Propulsion Laboratory, MC 264-767, 4800 Oak Grove Drive, Pasadena, CA 91109.
[2] Center for Radiophysics and Space Research, Cornell University, Space Sciences Building, Ithaca, NY 14853.
[3] Department of Astronomy, Ohio State University, 140 West 18th Avenue, Columbus, OH 43210; sellgren@astronomy.ohio-state.edu.
[4] Harvard-Smithsonian Center for Astrophysics, 60 Garden Street, Cambridge, MA 02138.
[5] Steward Observatory, University of Arizona, Tucson, 933 North Cherry Avenue, AZ 85721.
[6] *Spitzer* Science Center, Infrared Processing and Analysis Center, California Institute of Technology, Pasadena, CA 91125.

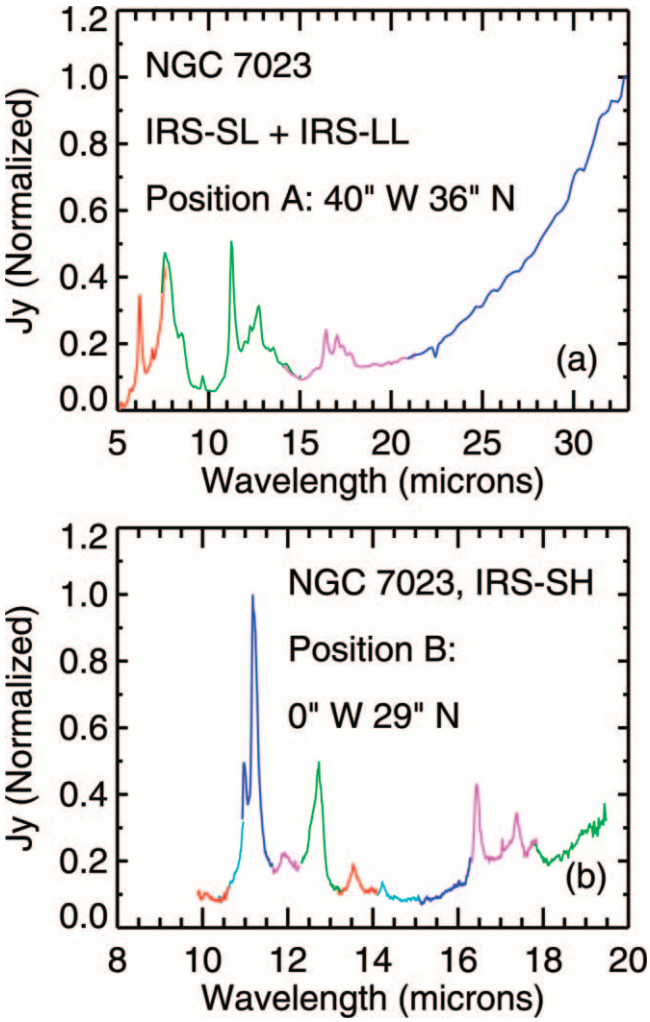

FIG. 3.—(*a*) Combined 5–33 μm normalized spectrum ($R = 60$–130) of position A in NGC 7023. We combined SL2 (5.1–7.6 μm; *red*), SL1 (7.5–15.1 μm; *green*), LL2 (14.0–21.1 μm; *magenta*), and LL1 (20.9–32.9 μm; *blue*) spectra. No scaling was done between SL2 and SL1. LL2 and LL1 were multiplied by factors of order ~2–3, after scaling by the beam size, in order to match SL1. (*b*) Normalized SH spectrum (9.9–19.4 μm; $R = 600$) of position B in NGC 7023, extracted from the entire entrance slit ($4\farcs7 \times 11\farcs3$). The spectrum is a composite of 11 orders, with substantial overlap between each. Relative uncertainty in the flux calibration between orders is ~7%. Adjacent orders are shown in contrasting colors.

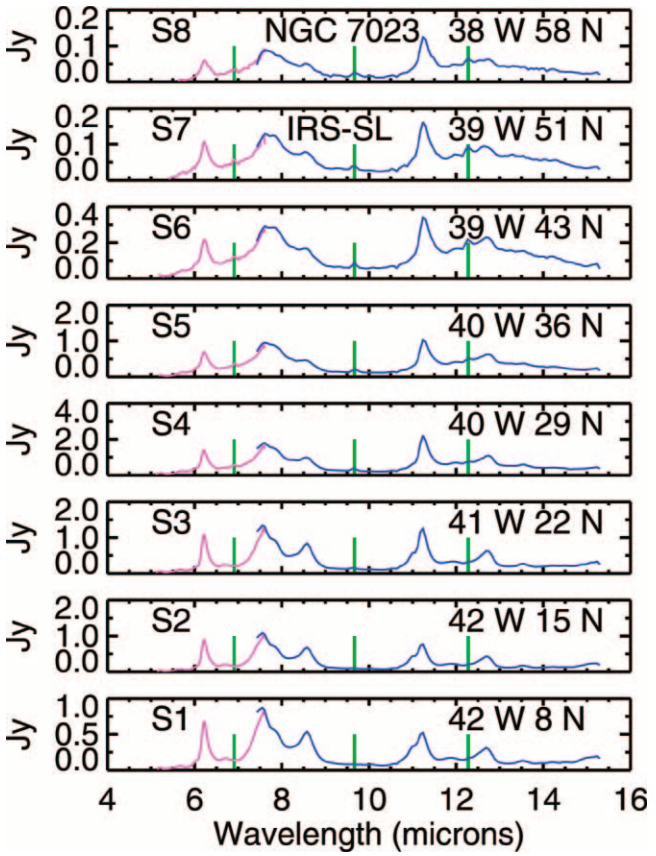

FIG. 4.—Long-slit SL ($R = 60$–130) spectra of NGC 7023. We extracted and combined SL2 (second-order; 5.1–7.6 μm) and SL1 (first-order; 7.5–15.1 μm) spectra at eight spatial locations, with a $7\farcs2 \times 3\farcs6$ box. No scaling was done; SL1 and SL2 agree well at overlapping wavelengths. The absolute flux uncertainty in SL is 25%. The *y*-axis is flux density (in janskys). The panel for each of the spectra S1 (*bottom to top*), S2, S3, S4, S5, S6, S7, and S8 is labeled with the offset of the spectrum, from HD 200775, in arcseconds, and the wavelengths of the H_2 lines 0–0 S(5) 6.91 μm, 0–0 S(3) 9.66 μm, and 0–0 S(2) 12.28 μm are marked (*vertical lines*).

and SL2 are uncertain by 25%, yet the relative agreement between them is much better than this factor. The SL and LL spectra were not expected to match, and we had to divide the LL2 and LL1 spectra by factors of ~2–3, after correction for beam size, to get all spectral segments to match. We emphasize that this composite spectrum of position A shows qualitatively the spectral features observed in this nebular region, and should *not* be used for quantitative analysis. The brightest spectral emission features seen in the spectrum are the AEFs at 6.2, 7.7, 8.6, 11.3, and 12.7 μm. Weaker emission features are also present, both spectrally resolved emission features and unresolved H_2 emission lines.

Figure 3*b* shows our SH spectrum (9.9–19.4 μm) at position B. Moutou et al. (2000) and Van Kerckhoven et al. (2000) have observed this wavelength region in NGC 7023 at a similar resolution but a different spatial position, using the SWS spectrometer on the *Infrared Space Observatory*, at a lower signal-to-noise ratio. Position A is near the H_2-emitting northwest filament, while position B is in a region with little H_2 emission (Lemaire et al. 1996). These two positions sample different physical conditions, yet show similar spectra. The higher spectral resolution of our SH spectrum (Fig. 3*b*) allows us to easily distinguish between unresolved emission lines, such as the 0–0 S(1) H_2 line at 17.03 μm, and resolved emission features, such as the adjacent 17.4 μm feature. Weak emission features that are barely spectrally resolved in Figure 3*a* are clearly resolved in Figure 3*b*.

One of the great strengths of *Spitzer* is the multiplex advantage, and the ability to discern spectral and spatial differences, of the long-slit spectrographs SL and LL. In Figure 3 we present the results from our long-slit SL observations. The AEFs are the brightest spectral features at all positions. We detect, in SL spectra closest to the star (S1–S4), the split between the 7.6 and 7.8 μm features that mainly comprise the "7.7" μm AEF (Fig. 3).

The 11.0 μm feature is clearly separated from the 11.3 μm AEF in Figure 3*b*. In Figure 4 we can observe the 11.0 μm feature blended with the 11.3 μm AEF in the SL spectra closest to the star (S1–S3). This blend, and its spatial variations, causes the 11.3 μm AEF to appear to decrease in FWHM and shift to longer wavelengths with increasing distance, d_*, from the star.

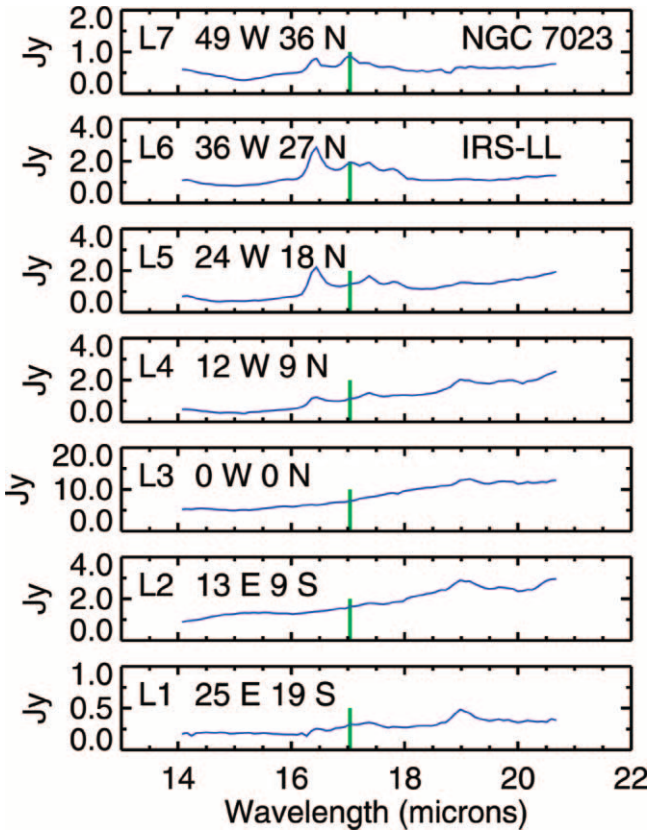

FIG. 5.—Long-slit LL2 (14.0–21.1 μm; $R = 60-130$) spectra of NGC 7023, extracted at seven spatial positions, each with a $15\farcs3 \times 10\farcs6$ box. The *y*-axis is flux density (in janskys). The absolute flux uncertainty in LL2 is 25%. The panel for each of the spectra L1 *(bottom to top)*, L2, L3, L4, L5, L6, and L7 is labeled with the offset of the spectrum, from HD 200775, in arcseconds, and the wavelength of the H_2 line 0–0 *S*(1) 17.03 μm is marked (*vertical line*). Spectrum L3 is HD 200775.

Figure 5 illustrates our LL2 spectra (14.0–21.1 μm) along the long slit of IRS-LL. Figure 5, together with Figure 3, demonstrate that longward of the five bright AEFs, there continues to be complex spectral structure. Most prominent in Figure 5 is an emission feature at 16.4 μm northwest of the star (L4–L7). Figure 5 also illustrates emission features northwest of the star, at 15.8, 17.4, and 17.8 μm. These features to the northwest are confirmed by the SL+LL spectrum of position A (Fig. 3*a*) and the SH spectrum of position B (Fig. 3*b*). Figure 5 also shows an emission feature both southeast and northwest of the star at 19.0 μm. Figures 3, 4, and 5 yield abundant evidence of pure rotational lines of H_2, marked on Figures 4 and 5. Fuente et al. (1999, 2000) have previously studied pure rotational lines of H_2 in NGC 7023.

Figures 3, 4, and 5 all show a faint but nonzero continuum, observed at 5–20 μm, in addition to spectral features and lines. This continuum emission is also detected spectroscopically at 2–4 μm in NGC 7023 (Sellgren et al. 1983; Martini et al. 1999), along with a strong 3.3 μm AEF and plateau of emission at 3.2–3.6 μm. These spectra demonstrate clearly that the emission in the IRAC 3.6 μm filter (3.2–3.9 μm) in NGC 7023 (Fig. 1) is due to a mix of this continuum emission with the 3.3 μm AEF and its accompanying 3.2–3.6 μm plateau emission.

Sellgren et al. (1983) and Sellgren (1984) proposed that the 2–5 μm continuum in NGC 7023 and other similar RNe is due to nonequilibrium thermal emission from tiny grains ($\sim$1 nm),

TABLE 1

NEW INFRARED EMISSION FEATURES

λ_c (μm)	Positions Detected[a]
6.7	S1–3
10.1	B, S1–3
15.8	A, L6–7
17.4	A, B, L4–6
19.0	L1–5

[a] Positions where features are detected. The nebular offset from HD 200775 of each position is labeled in Fig. 3 (positions A and B), Fig. 4 (positions S1–S8), and Fig. 5 (positions L1–L7).

stochastically heated to high temperatures ($\sim$1000 K) for a brief time by single stellar photons. The IRAC 4.5 μm filter covers 4.0–5.0 μm, a region in which no significant PAH features have been identified. We believe, therefore, that the emission within the IRAC 4.5 μm filter is completely due to this tiny grain continuum emission. The IRAC 8.0 μm filter covers 6.5–9.3 μm. Figures 3*a* and 4 clearly demonstrate that the IRAC 8.0 μm filter is dominated by AEF emission at 7.7 and 8.6 μm.

The 20–33 μm spectrum of position A (Fig. 3a) shows a strong rise to longer wavelengths, producing the emission in the 24 μm MIPS images (Fig. 2). *IRAS* 25 μm observations of the RN 23 Tau (Castelaz et al. 1987) agree with predictions (Draine & Anderson 1985) that emission in this wavelength region is due to stochastically heated tiny grains. We expect this to be true of NGC 7023 as well.

4. DISCUSSION

4.1. *Discoveries of New Emission Features*

We have discovered new ISM emission features at 6.7, 10.1, 15.8, 17.4, and 19.0 μm in NGC 7023. These features are spectrally resolved and so are not atomic or molecular emission lines. All five new features are observed in multiple positions with SH, SL, or LL, giving confidence that they are not instrumental artifacts. The 10.1 μm feature seen in SL and the 17.4 μm feature seen in LL are both clearly detected in SH. These ISM spectral emission features are among the first spectroscopic discoveries made by *Spitzer*.

Currently, these features have no identification. Possible identifications could include PAH bands, such as C—H out-of-plane bending modes for 10.1 μm (Hony et al. 2001), or C—C—C bending modes for 15.8, 17.4, and 19.0 μm (Van Kerckhoven et al. 2000). The spectral structure at 6–9 μm is quite complicated, with only tentative identifications for well-known features (Peeters et al. 2002), making it difficult to predict whether the 6.7 μm feature might fit into the PAH model. Alternate possibilities, particularly at the longer wavelengths, include nanoparticles ($\sim$1 nm) of a specific mineral composition. For instance, Molster et al. (2001) identify a mixture of PAH species between 3 and 12 μm and various crystalline and amorphous silicates beyond 18 μm in the spectrum of the planetary nebula NGC 6302. Other mineral species, such as simple metal oxides or other combinations of abundant refractory materials, also remain to be explored.

4.2. *Spatial Variations in Spectral Features*

We observe marked changes in spectral features across NGC 7023. The nebula southeast of the star is where the new

19.0 μm feature is brightest. To the northwest of HD 200775, the 19.0 μm feature fades and the 16.4 μm feature becomes the brightest feature in our LL2 spectra.

Our long-slit observations show that the relative strengths of various pairs of emission features vary with d_*. We consider feature pairs observed in the same order and module of IRS and find that the ratios 7.8/7.6, 7.4/7.6, 11.3/11.0, and 11.3/7.7 μm increase with increasing d_*.

One of the most marked spectral changes is an apparent weakening of the 8.6 μm AEF with increasing d_*. Uchida et al. (2000) and Cesarsky et al. (2000) observe this same phenomenon in other RNe, and attribute it to a broadening of the 7.7 μm AEF with increasing d_*. We confirm that the 7.7 μm AEF is broader, and we also find that its central wavelength increases with increasing d_*. This suggests that the wing of the 7.8 μm feature, as it grows in strength relative to the 7.6 μm feature, steadily overwhelms the 8.6 μm AEF until it is barely visible. The 6.2 μm AEF, like the 7.7 μm AEF, appears broader at larger d_*. The equivalent width of the 6.2 μm AEF also markedly decreases with increasing d_*.

Another striking spectral variation with d_* is the changes in the 11–14 μm region. Close to the star, distinct features at 11.0, 11.3, 12.0, and 12.7 μm can be distinguished. Far from the star, this spectral region can only be fitted by a blend of the 11.3 μm AEF and a broad bump of emission, centered at 12.5 μm and having a FWHM of 2.0 μm. This broad 12.5 μm feature increases with increasing d_*, and is not observed close to the star. The same 11–14 μm behavior with increasing d_* has been observed in the RN Ced 201 (Cesarsky et al. 2000).

4.3. *Imaging*

In the inner regions of the nebula, we find strong similarities between the IRAC 4.5 μm continuum image and the IRAC 8.0 μm AEF image. The ring of emission between HD 200775 and the northwest filaments is real and is observed in ground-based images of the 3.3 μm AEF (An & Sellgren 2003).

On the largest scales ($\sim 6'$, or ~ 0.8 pc), our 4.5, 8.0, and 24 μm images show an hour-glass shape, containing little IR emission, which is clearly outlined by a narrow rim of IR emission. The filaments within $\sim 1'$ of HD 200775 define the narrow waist of the hourglass shape. This spatial structure has been observed before, in 1–0 ^{13}CO, 2–1 ^{12}CO, and 3–2 ^{13}CO (Gerin et al. 1998; Fuente et al. 1998), at $10''$–$20''$ resolution. Watt et al. (1986) and Fuente et al. (1998) have argued that the hourglass shape is the fossil remnant of a bipolar outflow from the Herbig Be star HD 200775, implying that the large-scale mid-IR emission outlines the walls of the cavity produced by the earlier outflow.

Note added in manuscript.—After this paper was completed, M. Jura of UCLA kindly pointed out to us that the positions and widths of the new 17.4 and 19.0 μm features agree rather well with those of the two lower frequency vibrational transitions of the C_{60} molecule (Frum et al. 1991). It is not possible to establish detection of interstellar C_{60} on the basis of the data in the present paper, but we will explore this potential identification with additional observations and analysis. Note, however, that Moutou et al. (1999) have set limits on the abundance of C_{60} and C_{60}^+ in NGC 7023 based on nondetection of the two higher frequency vibrational transitions between 7 and 9 μm.

We thank the people whose dedicated work made the *Spitzer Space Telescope* a reality (see Werner et al. 2004). This work is based on observations made with the *Spitzer Space Telescope*, which is operated by the Jet Propulsion Laboratory, California Institute of Technology, under NASA contract 1407. Support for this work was provided by NASA through contract 1257184, issued by JPL/Caltech. K. S. thanks the JPL Center for Long-Wavelength Astrophysics for support.

REFERENCES

Allamandola, L. J., Tielens, A. G. G. M., & Barker, J. R. 1985, ApJ, 290, L25
An, J. H., & Sellgren, K. 2003, ApJ, 599, 312
Castelaz, M. W., Sellgren, K., & Werner, M. W. 1987, ApJ, 313, 853
Cesarsky, D., Lequeux, J., Ryter, C., & Gerin, M. 2000, A&A, 354, L87
Draine, B. T., & Anderson, N. 1985, ApJ, 292, 494
Duley, W. W., & Williams, D. A. 1981, MNRAS, 196, 269
Fazio, G. G., et al. 2004, ApJS, 154, 10
Frum, C. I., Engelman, R., Hedderich, H. G., Bernath, P. F., Lamb, L. D., & Huffman, D. R. 1991, Chem. Phys. Lett. 176, 504
Fuente, A., Martín-Pintado, J., Rodríguez-Fernández, N. J., Cernicharo, J., & Gerin, M. 2000, A&A, 354, 1053
Fuente, A., Martín-Pintado, J., Rodríguez-Fernández, N. J., Rodríguez-Franco, A., de Vicente, P., & Kunze, D. 1999, ApJ, 518, L45
Fuente, A., Martín-Pintado, J., Rodríguez-Franco, A., & Moriarty-Schieven, G. D. 1998, A&A, 339, 575
Gerin, M., Phillips, T. G., Keene, J., Betz, A. L., & Boreiko, R. T. 1998, ApJ, 500, 329
Gordon, K. D., et al. 2004, PASP, submitted
Higdon, S., et al. 2004, PASP, submitted
Hony, S., Van Kerckhoven, C., Peeters, E., Tielens, A. G. G. M., Hudgins, D. M., & Allamandola, L. J. 2001, A&A, 370, 1030
Houck, J. R., et al. 2004, ApJS, 154, 18
Léger, A., & Puget, J. L. 1984, A&A, 137, L5
Lemaire, J. L., Field, D., Gerin, M., Leach, S., Pineau des Forêts, G., & Rouan, D. 1996, A&A, 308, 895
Martini, P., Sellgren, K., & DePoy, D. L. 1999, ApJ, 526, 772
Molster, F. J., et al. 2001, A&A, 372, 165
Moutou, C., Sellgren, K., Verstraete, L., & Léger, A. 1999, A&A, 347, 949
Moutou, C., Verstraete, L., Léger, A., Sellgren, K., & Schmidt, W. 2000, A&A, 354, L17
Peeters, E., Hony, S., Van Kerckhoven, C., Tielens, A. G. G. M., Allamandola, L. J., Hudgins, D. M., & Bauschlicher, C. W. 2002, A&A, 390, 1089
Rieke, G. H., et al. 2004, ApJS, 154, 25
Sellgren, K. 1984, ApJ, 277, 623
Sellgren, K., Werner, M. W., & Dinerstein, H. L. 1983, ApJ, 271, L13
Uchida, K. I., Sellgren, K., Werner, M. W., & Houdashelt, M. L. 2000, ApJ, 530, 817
van den Ancker, M. E., Thé, P. S., Tjin A Djie, H. R. E., Catala, C., de Winter, D., Blondel, P. F. C., & Waters, L. B. F. M. 1997, A&A, 324, L33
Van Kerckhoven, C., et al. 2000, A&A, 357, 1013
Watt, G. D., Burton, W. B., Choe, S.-U., & Liszt, H. S. 1986, A&A, 163, 194
Werner, M. W., et al. 2004, ApJS, 154, 1

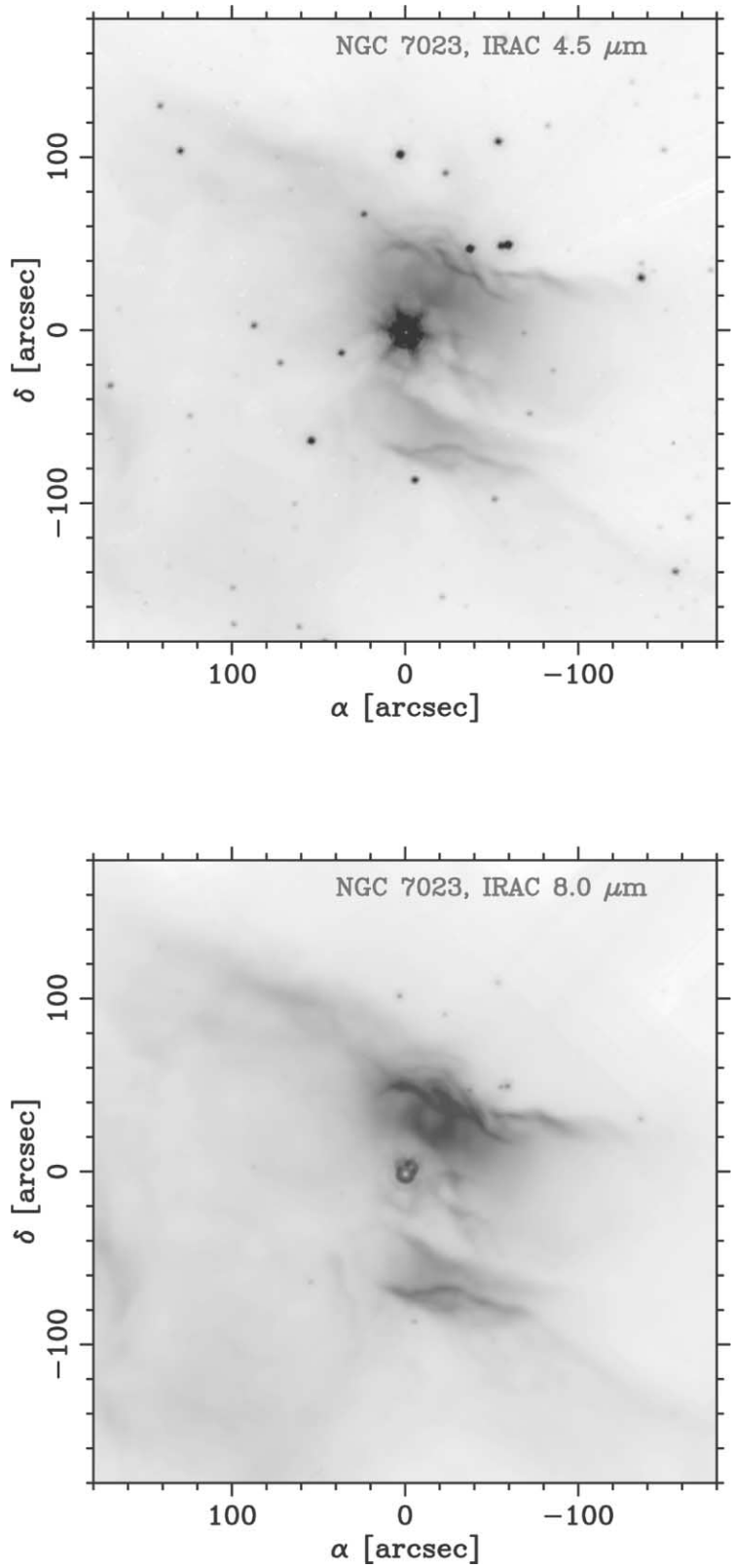

FIG. 1.—IRAC images of the central $6' \times 6'$ of the RN NGC 7023, at 4.5 μm (*top*) and 8.0 μm (*bottom*). NGC 7023 spectra show that the IRAC 4.5 μm filter is continuum emission and the IRAC 8.0 μm filter is primarily AEF emission. Both observations were made with the 12 s high dynamic range mode, consisting of a 1.2 s exposure for observing bright field stars, followed by a 10.4 s exposure for detecting the low surface brightness nebular emission. Even in this mode, the central star, HD 200775, is saturated in both images. North is up, and east is to the left.

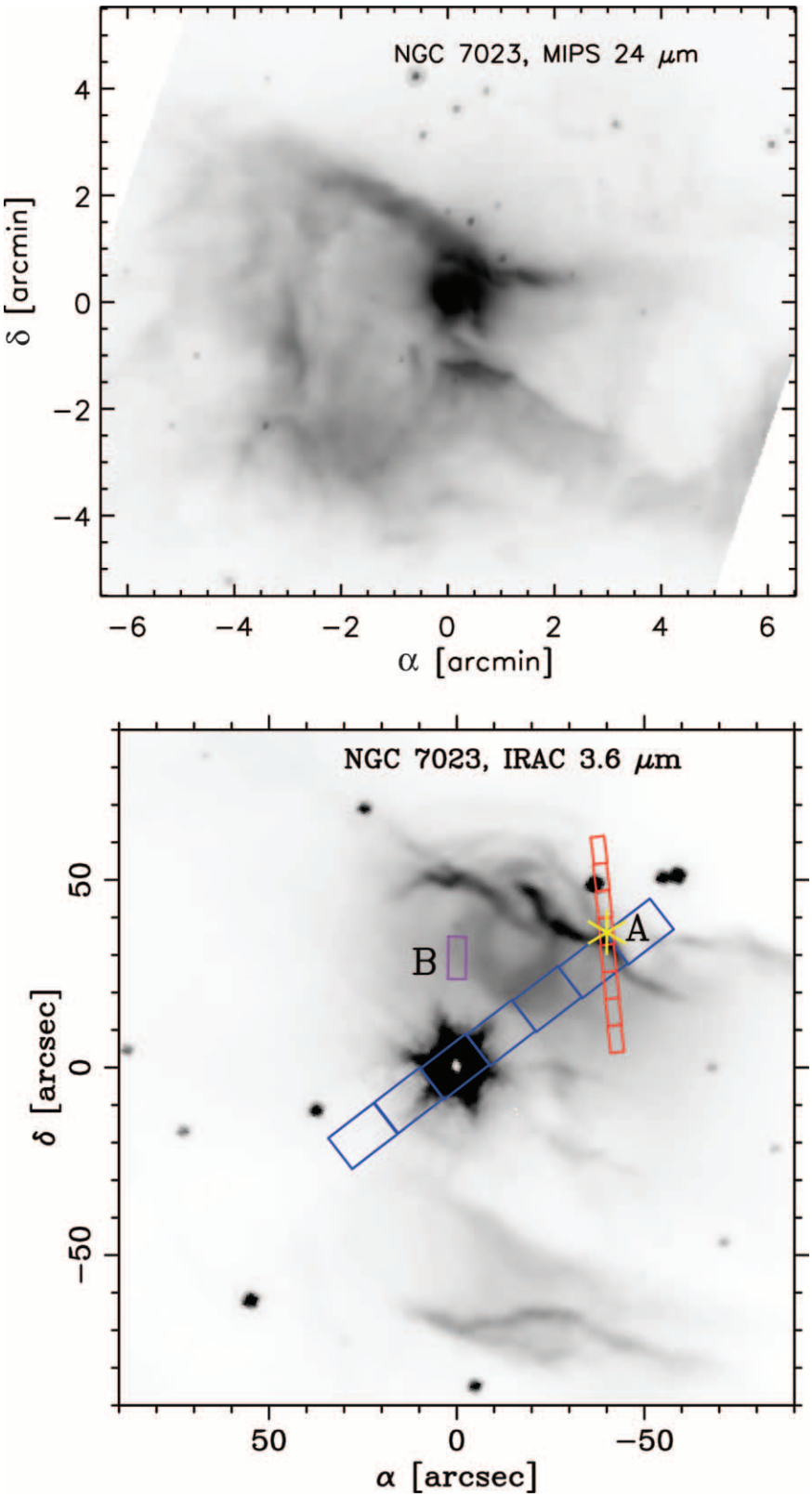

FIG. 2.—MIPS image of the central $\sim 12' \times \sim 10'$ of NGC 7023 at 24 μm (*top*) and IRAC image of the central $\sim 3' \times \sim 3'$ region at 3.6 μm (*bottom*). We illustrate how the IRS slits overlay different parts of the central regions of our 3.6 μm IRAC image, which is our highest spatial resolution *Spitzer* image. We extracted and combined SL2 and SL1 spectra at eight spatial locations. Spectrum S1 (42″ west, 8″ north) is closest to the star and spectrum S8 (38″ west, 58″ north) is farthest from the star. We extracted LL2 spectra at seven spatial positions. Offsets range from 25″ east, 19″ south (spectrum L1) to 49″ west, and 36″ north (spectrum L7). Spectrum L3 is HD 200775. Position A (the intersection of SL and LL) and position B (the slit location for SH) are marked. North is up, and east is to the left.